IJRCS

International Journal of Robotics and Control Systems
Vol. 6, No. 2, 2026, pp. 1617-1636
ISSN 2775-2658
http://pubs2.ascee.org/index.php/ijrcs

ASCEE

The Component Placement Process in Surface Mount Technology Based on Coordinate Calculation Equations

Nguyen Trung Nhan [a,1], Thanh Quyen Ngo [a,2,*], Phan Quoc Thai Tran [a,3], Binh Minh Lam [a,4], Thi Tu Uyen Hoang [a,5], Ngoc Hoi Le [a,6], Thanh Hai Tran [b,7]

[a] Faculty of Electrical Engineering Technology, Industrial University of Ho Chi Minh City, Ho Chi Minh City 700000, Vietnam
[b] Office of Planning and Investment, Industrial University of Ho Chi Minh City, Ho Chi Minh City 700000, Vietnam
[1] nguyentrungnhan@iuh.edu.vn; [2] ngothanhquyen@iuh.edu.vn; [3] tpquocthai2203@gmail.com;
[4] lambinhminh@iuh.edu.vn; [5] hoangthituuyen@iuh.edu.vn; [6] lengochoi@iuh.edu.vn; [7] tranthanhhai@iuh.edu.vn
* Corresponding Author

ARTICLE INFO

Article history
Received November 19, 2025
Revised January 19, 2026
Accepted May 28, 2026

Keywords
SMT Placement Accuracy;
Coordinate Calculation;
Pick-and-Place Machine;
Mathematical Modeling;
Electronics Manufacturing

ABSTRACT

Accurate component placement in Surface Mount Technology (SMT) is essential for assembly yield and long-term product reliability. In practice, placement accuracy is often degraded by fixture offsets, vibration, and feeder/nozzle variability, while many optimization approaches remain predominantly offline and therefore cannot directly compensate for runtime deviations. This paper proposes a generalized coordinate calculation framework based on linear transformation principles, implemented in a PLC-controlled three-axis pick-and-place prototype. Using a small set of reference parameters, the proposed method generates consistent coordinates for passive components, ICs, and feeders and supports fast recalculation when the PCB reference origin changes. Experimental validation was conducted on 62 PCB assemblies, achieving a placement success rate of 91.94% (57/62). For all successful boards, the placement deviation remained within the predefined tolerance window (±0.2 mm), and observed failures were attributable to hardware issues (feeder misfeed and vacuum loss) rather than the coordinate model. The research contribution of this paper is a practical, real-time adaptable alternative for coordinate programming in SMT pick-and-place systems, with future work focusing on vision-assisted referencing, hardware reliability improvements, and benchmarking against offline optimization methods on larger PCB layouts.

1. Introduction

In modern electronics manufacturing, automated component placement machines employing Surface Mount Technology (SMT) are widely utilized [1]–[3], playing a pivotal role in ensuring placement accuracy and assembly efficiency compared to conventional through-hole technology [4]–[6]. Nevertheless, one of the most critical challenges in SMT systems lies in achieving highly precise component coordinate calculation with minimal error [7], particularly for ultra-miniaturized components. Accurate coordinate determination not only influences soldering quality but also directly impacts the reliability and lifespan of the final product [8], [9].

In the current context, where the integration density of printed circuit boards (PCBs) continues to increase [10]–[13], the precision requirements for the pick-and-place process have advanced beyond the micrometer scale, approaching the nanometer level for certain high-end electronic devices [14]. This trend makes coordinate determination and trajectory optimization of the placement nozzle a crucial issue for manufacturers. Furthermore, the rapid growth of the Internet of Things (IoT), mobile devices, and embedded systems has created a strong demand for compact PCBs densely populated with complex components, thereby introducing additional challenges to the assembly process [15]–[19].

The assembly of a complete printed circuit board (PCB) requires multiple stages, including adhesive application, component pick-and-place, reflow soldering, and inspection [20], [21]. Among these, the SMT pick-and-place process is the most critical stage, as it demands near-perfect accuracy in positioning each component on the PCB [22]. Therefore, determining component coordinates using mathematical equations is essential for improving both placement accuracy and production reliability. In present, various approaches have been introduced to determine placement paths or component coordinates, such as Heuristic algorithms [23]–[26], Genetic algorithms [27]–[31], and Ant Colony algorithms [32]–[36], all aiming to enhance the accuracy of electronic component assembly.

However, evolutionary and metaheuristic algorithms primarily optimize parameters in an offline manner, meaning coordinate optimization must be completed prior to actual operation. This constitutes their major limitation, since in practical manufacturing environments, component positions may shift due to machine vibrations, fixture tolerances, or mechanical interactions, which can reduce placement accuracy and render offline optimization ineffective [37]–[41]. Hence, there remains a clear research gap in developing generalized coordinate calculation solutions that can dynamically adapt to positional variations under real operating conditions.

In addition to optimizing placement efficiency through feeder allocation and nozzle selection, the optimization of the assembly process by means of coordinate calculation is equally important for improving both performance and quality [25], [42]–[46]. To address these gaps, the present research develops a generalized mathematical model to accurately determine component coordinates and optimize placement paths in SMT systems, applied to a 3.3V low-voltage circuit Fig. 1. The proposed method reduces coordinate errors and shortens assembly time by enabling systematic coordinate generation and flexible adjustment of PCB positions according to actual machine conditions. As a result, this approach overcomes key limitations of previous evolutionary algorithms and provides a practical foundation for improving SMT placement performance in real production environments.

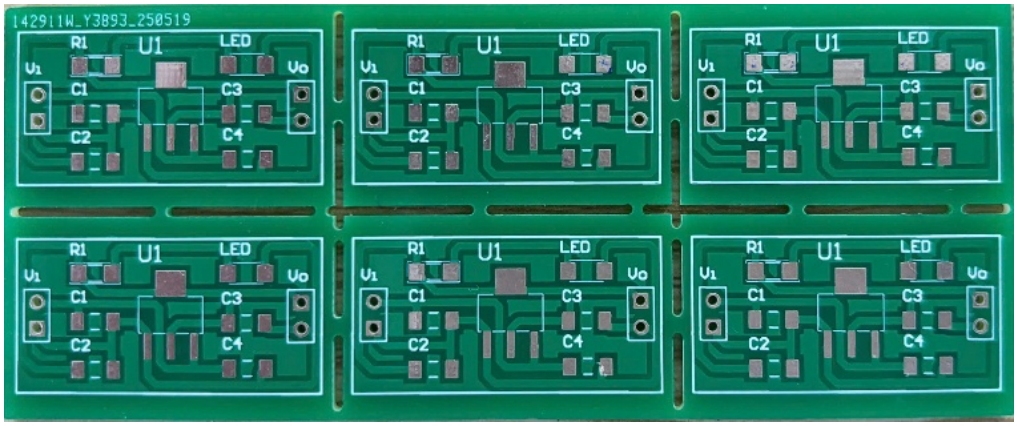

Fig. 1. Printed circuit board (PCB) used for processing

To address these gaps, the present research develops a generalized mathematical model to accurately determine component coordinates and optimize placement paths in SMT systems, applied to a 3.3V low-voltage circuit Fig. 1. This approach reduces errors and shortens assembly time. Furthermore, the proposed equations allow operators to flexibly adjust PCB positions according to the actual machine conditions, overcoming the limitations of previous evolutionary algorithms.

2. Component Coordinate Calculation on the PCB

The proposed method aims to reduce manual coordinate entry by generating all placement coordinates from a limited set of reference parameters. At runtime, the operator (or the system) provides a PCB reference point in machine coordinates (datum) and a small set of spacing parameters derived from the PCB layout. The algorithm then calculates coordinates for all placement points and feeder pickup locations.

Conceptually, the mapping from PCB reference coordinates to the machine coordinate system can be interpreted as a linear transformation dominated by translation and (if needed) a small planar rotation. In our PLC implementation, the mapping is realized using straight-line relationships of the form $y = ax + b$ [47], which provides an efficient arithmetic form for coordinate generation and fast recalculation when the datum changes.

Fig. 2 illustrates the XY motion axes (horizontal plane), driven by two 200 W servo motors, each directly coupled to a 600 mm travel ball screw, a design that ensures high positioning accuracy [48]–[52]. In addition, the Z axis (vertical axis) controls the pick-and-place operations, driven by a 100 W servo motor combined with a belt-drive mechanism. This configuration allows the synchronized movement of two vacuum nozzles in a fast and flexible manner. The coordinate system employed in this study is depicted in Fig. 3, it provides a visual representation of the two key coordinate systems utilized throughout this study: the machine coordinate system, which defines the absolute working envelope of the equipment, and the PCB reference system, which is used to locate components relative to the board itself.

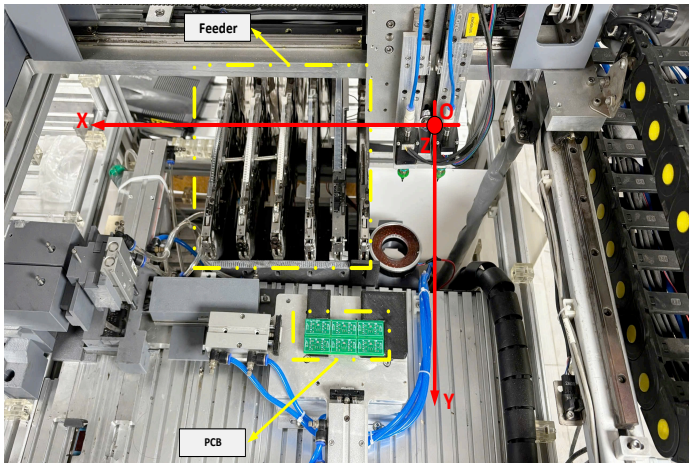

Fig. 2. Experimental SMT model

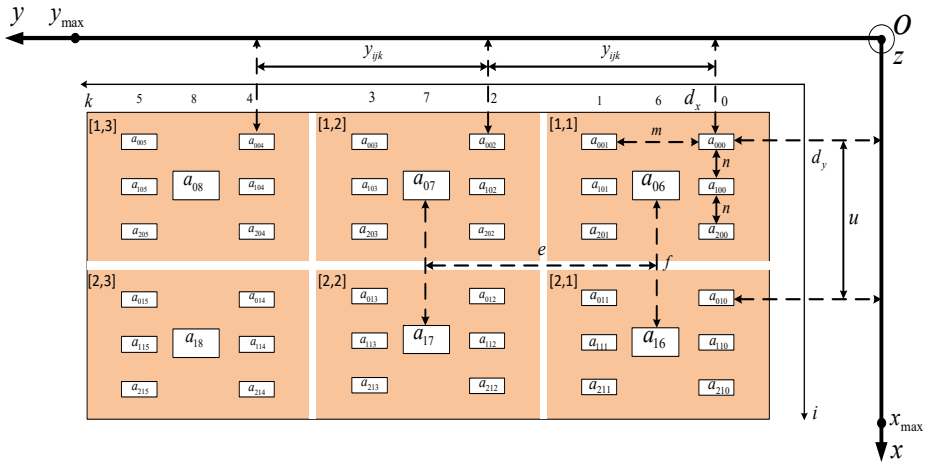

Fig. 3. Diagram of the machine coordinate system relative to the PCB and component position

where i is the iteration index along the *x-axis*; j is the number of components with respect to i; k is the iteration index of components in column order along the $y-axis$; d_x and d_y is the current coordinate of the component to be placed at the first position on the PCB (a_{000}); x_{max} and y_{max} denotes the travel limit of the ball screw; y_{ij} is the spacing between components in successive PCBs (between the $2k-th$ and $(2k+1)-th$ boards); x_j is the spacing between two consecutive components with respect to i; n is the spacing between two components along the $x-axis$ on a single PCB; m is the spacing between two components along the *y-axis* between two PCBs; e is the spacing between two ICs along the *y-axis*; f is the spacing between two ICs along the $x-axis$; and u is the spacing between two components along the *x-axis* between two PCBs.

2.1. Component Coordinates

To ensure the generality and reproducibility of the results, the current prototype is constructed based on the following assumptions:

1) **Rigid PCB assumption:** The printed circuit board (PCB) is considered perfectly rigid during pick-and-place operations. Therefore, the influence of board warpage and any warpage compensation mechanism is not included in the present study.
2) **Negligible scale effect:** Scale effects are neglected (i.e., the scale factor is approximately 1). Hence, the dominant deviations in practical operation are expected to originate mainly from translational displacement and rotational errors, which may be introduced by fixture inaccuracy and reference misalignment.
3) **Placement accuracy criterion:** The placement accuracy is evaluated using a predefined tolerance window of ± 0.2 mm. In the context of PCB footprint/land-pattern tolerance analysis, the IPC-7351 standard defines the placement tolerance parameter *P*, which is widely adopted as a reference in engineering practice.
4) **Unified linear representation:** To improve both generality and computational efficiency, the coordinates of components handled by the primary nozzle and the secondary nozzle are expressed using a general linear equation.

Based on this framework, the study plans the overall coordinates of all objects, such as discrete components, ICs, and feeders, on the Oxy plane. These are then converted into the form of coordinates represented by the general linear equation to facilitate programming, operation, and maintenance in subsequent implementation stages.

2.1.1. Linear Transformation Model for Component Mapping

The coordinate mapping is derived from the straight-line equation, where the slope coefficient a a is computed from two reference points:

$$a = \frac{y_2 - y_1}{x_2 - x_1} = \frac{y_{max} - d_y}{x_{max} - d_x} \quad (1)$$

Here, $x_1 = d_x$ and $y_1 = d_y$ are the current coordinates of the component to be placed at the first position of the PCB; $x_2 = x_{\max}$and $y_2 = y_{\max}$ represent the travel limits of the ball screw axes; y_{ij} denotes the spacing of components between the $2k-th$ and $(2k+1)$-th boards, while x_j refers to the spacing between two consecutive components with respect to index i, defined as:

$$x_j = \begin{cases} 0, & \text{when } j = 0 \\ u, & \text{when } j > 0 \end{cases}$$

Here, u denotes the spacing between two components along the x-axis across two printed circuit boards. The definitions are as follows: i represents the number of iterations along the x-axis, and j is the component index with respect to i.

2.1.2. Slope Coefficients for the First Column ($k = 0$)

To establish the coordinate coefficients for component placement, the slope coefficient a a is first derived for the first PCB column ($k = 0$) at successive component indices $i = 0, 1, 2$.

For the first component placement at the first column ($i = 0, k = 0$):

$$\begin{cases} a_{00} = \dfrac{y_{\max} - d_y}{x_{\max} - x_0 - 0n - d_x} \\ a_{01} = \dfrac{y_{\max} - d_y}{x_{\max} - x_1 - 0n - d_x} \end{cases} \tag{2}$$

For the second component placement at the first column ($i = 1, k = 0$):

$$\begin{cases} a_{10} = \dfrac{y_{\max} - d_y}{x_{\max} - x_0 - 1n - d_x} \\ a_{11} = \dfrac{y_{\max} - d_y}{x_{\max} - x_1 - 1n - d_x} \end{cases} \tag{3}$$

For the third component placement at the first column ($i = 2, k = 0$):

$$\begin{cases} a_{20} = \dfrac{y_{\max} - d_y}{x_{\max} - x_0 - 2n - d_x} \\ a_{21} = \dfrac{y_{\max} - d_y}{x_{\max} - x_1 - 2n - d_x} \end{cases} \tag{4}$$

From (2)–(4), the general expression of the slope coefficient for the component coordinates is defined as follows:

$$a_{ij} = \frac{y_{max} - d_y}{x_{max} - x_j - i \times n - d_x} \tag{5}$$

where $i = 0, 1, 2$; $j = 0, 1, 2$; and n denotes the spacing between two consecutive components along the x-axis on a single PCB.

2.1.3. Extension to Multi-Column PCB Arrangement

Equation (5) only represents the slope coefficient a of the component coordinates for one column. However, since a printed circuit board (PCB) contains six different modules, we introduce k as the iteration index of components along the y-axis columns, as illustrated in Fig. 3. Accordingly, the slope coefficient a of the component coordinates on the PCB, at the first component iteration of the first column ($i = 0, k = 0$), is determined as follows:

$$\begin{cases} a_{000} = \dfrac{y_{\max} - \eta y_{ijk} - d_y}{x_{\max} - x_0 - 0n - d_x} \\ a_{010} = \dfrac{y_{\max} - \eta y_{ijk} - d_y}{x_{\max} - x_1 - 0n - d_x} \end{cases} \tag{6}$$

Based on the rules derived for (5), the generalized form of (6) can be expressed as follows:

$$a_{\text{ijk}} = \frac{y_{\max} - \eta y_{ijk} - d_y}{x_{\max} - x_j - i \times n - d_x} \tag{7}$$

where η the amplification factor with respect to the repetition index k and the coordinates of the $i - th$ column in the $k - th$ sequence are defined in two cases as in Section 2.1.4.

2.1.4. Even–Odd Indexing Rule for

For even values of k $(2N)$, the a_{ijk} coefficient of the component coordinate system is determined as follows: $\eta = \frac{k}{2}$, and the slope coefficient is:

$$a_{\text{ijk(2N)}} = \frac{y_{\max} - \eta y_{ijk} - d_y}{x_{\max} - x_j - i \times n - d_x} \tag{8}$$

Conversely, for odd values of k $(2N+1)$, the a_{ijk} coefficient of the component coordinate system is determined as follows: $\eta = \frac{k-1}{2}$, and the slope coefficient becomes:

$$a_{\text{ijk(2N+1)}} = \frac{y_{\max} - \eta y_{ijk} - m - d_y}{x_{\max} - x_j - i \times n - d_x} \tag{9}$$

where $N = 0, 1, 2, 3$ ... is an integer; $k = 0, 1, 2, 3, 4, 5$ and m denotes the distance between two components along the y-axis between two printed circuit boards.

By substituting (8) and (9) into equation (1), the component coordinates are calculated as follows:

For even $k = 2N$:

$$y - (\eta y_{ijk} + d_y) = a_{\text{ijk(2N)}}\left[x - (x_j + i \times n + d_x)\right] \tag{10}$$

For odd $k = 2N + 1$:

$$y - (\eta y_{ijk} + m + d_y) = a_{\text{ijk(2N+1)}}\left[x - (x_j + i \times n + d_x)\right] \tag{11}$$

Equation (10) and (11) provide the final coordinate representation for component placement on the PCB, ensuring that the coordinate generation process remains scalable and systematically applicable across multiple PCB columns.

2.2. Component Coordinates of the IC:

After deriving the coordinate coefficients for component placement corresponding to $k = 0, 1, 2, 3, 4, 5$, this subsection extends the coordinate calculation framework to integrated circuits (ICs), which are arranged along the *y-axis* for $k = 6, 7, 8$. In this stage, the IC placement sequence follows the same transformation principle derived from (1), where the slope coefficient is recalculated to reflect the IC spacing and offset parameters.

2.2.1. Slope Coefficient Formulation for IC Placement

To determine the IC coordinate system, the slope coefficients are computed for each iteration index k. The derivations for $k = 6, k = 7$, and $k = 8$ are presented below.

At the iteration corresponding to $k = 6$:

$$\begin{cases} a_{06} = \dfrac{y_{\max} - \dfrac{m}{2} - 0e - d_y}{x_{\max} - \alpha - n - 0f - d_x} \\ a_{16} = \dfrac{y_{\max} - \dfrac{m}{2} - 0e - d_y}{x_{\max} - \alpha - n - 1f - d_x} \end{cases} \tag{12}$$

At the iteration corresponding to $k = 7$:

$$\begin{cases} a_{07} = \dfrac{y_{\max} - \dfrac{m}{2} - 1e - d_y}{x_{\max} - \alpha - n - 0f - d_x} \\ a_{17} = \dfrac{y_{\max} - \dfrac{m}{2} - 1e - d_y}{x_{\max} - \alpha - n - 1f - d_x} \end{cases} \tag{13}$$

At the iteration corresponding to $k = 8$:

$$\begin{cases} a_{08} = \dfrac{y_{\max} - \dfrac{m}{2} - 2e - d_y}{x_{\max} - \alpha - n - 0f - d_x} \\ a_{18} = \dfrac{y_{\max} - \dfrac{m}{2} - 2e - d_y}{x_{\max} - \alpha - n - 1f - d_x} \end{cases} \tag{14}$$

2.2.2. Generalized Expression of the IC Slope Coefficient

From (12)–(14), it can be observed that the slope coefficient varies systematically with respect to the IC index k. Therefore, a generalized form of the slope coefficient for IC placement is established as:

$$a_{jk} = \frac{y_{\max} - \dfrac{m}{2} - \beta e - d_y}{x_{\max} - \alpha - n - j \times f - d_x} \tag{15}$$

where β is the amplification factor with respect to k for $k > 5$, therefore, the coefficient β is defined as follows: $\beta = k - 6$; α is an arbitrary positive coefficient of the IC along the x-axis; e is the spacing between two ICs along the y-axis; and f is the spacing between two ICs along the x-axis.

2.2.3. Coordinate System Representation of IC Placement

Using the same rules employed to derive (10) and (11) for (15), the coordinate system of the IC is defined as follows:

$$y - (\frac{m}{2} + \beta e + d_y) = a_{jk}[x - (\alpha + n + j \times f + d_x)] \tag{16}$$

Equation (16) provides a generalized linear representation of the IC placement coordinates, ensuring that the coordinate generation remains consistent and scalable for different IC positions along the placement sequence.

3. Feeder Coordinates and System Operational Cycle

Fig. 4 illustrates the schematic diagram of the coordinate system and the motion cycle of the axis. The diagram defines several key parameters governing the pick-and-place sequence. Here, l denotes the sequence of motion trajectories. The index δ indicates the order of the feeders. The parameter d_f denotes the distance between consecutive feeders, and d_{f0} represents the distance from the origin to the first feeder (a_1).

The motion cycle is executed according to the following rule: the trajectory where l = 0 corresponds to the trajectory from the origin (O) to the position of feeder 5 supplying LED components (a_5). Odd values of l represent the return cycles to the feeder for component pickup. Conversely, even values of l represent the forward cycles where the head moves toward the designated placement positions on the PCB.

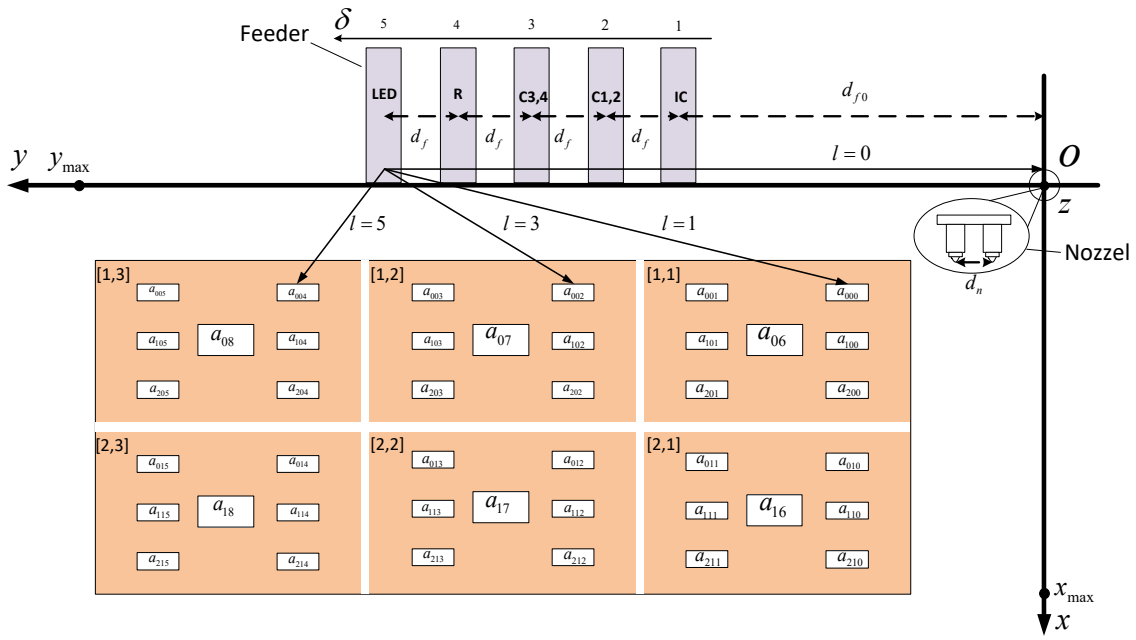

Fig. 4. Schematic diagram illustrating the feeder coordinates and the motion cycle of the axis

3.1. Feeder coordinates

In addition to the placement coordinates on the PCB, the pick-and-place process requires accurate pickup coordinates at the feeders. In the proposed framework, feeder pickup points are generated using the same linear relationship form employed for component coordinates. This ensures that feeder coordinate generation is consistent with the machine coordinate system and can be recalculated immediately when the datum point changes.

For the feeder supplying 5 (LED):

$$a_5 = \frac{y_{\max} - 4d_f - d_{f0}}{x_{\max}} \tag{17}$$

For the feeder supplying 4 (R):

$$a_4 = \frac{y_{\max} - 3d_f - d_{f0}}{x_{\max}} \tag{18}$$

For the feeder supplying 3 (C3 and C4):

$$a_3 = \frac{y_{\max} - 2d_f - d_{f0}}{x_{\max}} \tag{19}$$

For the feeder supplying 2 (C1 and C2):

$$a_2 = \frac{y_{\max} - d_f - d_{f0}}{x_{\max}} \tag{20}$$

For the feeder supplying 1 (IC):

$$a_1 = \frac{y_{\max} - 0d_f - d_{f0}}{x_{\max}} \tag{21}$$

Based on the rules for determining the coefficients in the generalized equations presented above, the generalized slope coefficient of the feeder coordinates is defined as follows:

$$a_\delta = \frac{y_{\max} - (\delta - 1)d_f - d_{f0}}{x_{\max}} \tag{22}$$

where δ denotes the feeder index; d_f represents the distance between two feeders; and d_{f0} is the distance from the home position to the first feeder.

By substituting the slope coefficient in (22) into (1), the feeder coordinates are defined as follows:

$$y - ((\delta - 1)d_f + d_{f0}) = a_\delta x \tag{23}$$

3.2. Coordinates of the Primary and Secondary Nozzles with Respect to the Component and Feeder Coordinates

This section describes the dual-nozzle configuration utilized for the pick-and-place operation, with its schematic layout presented in Fig. 5. Within this configuration, a key geometric parameter is the fixed distance between the centers of the primary and secondary nozzles, denoted as d_n. This inter-nozzle distance is a critical design constant that directly influences the kinematic calculations, the planning of motion trajectories, and ultimately, the efficiency and accuracy of concurrent component handling.

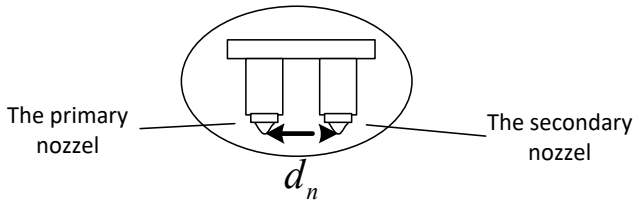

Fig. 5. Illustration of the dual nozzles and the distance between them

The primary nozzle is responsible for picking and placing components on the upper row of the printed circuit board (PCB), corresponding to $j = 0$. Meanwhile, the secondary nozzle handles the picking and placing of components on the lower row of the PCB, corresponding to $j = 1$. Accordingly, the equations describing the coefficients for all three coordinate systems (component, IC, and feeder) are reformulated as follows.

For the component coordinates, the coefficients of the primary and secondary nozzles are redefined as follows:

$$a_{\text{ijk(2N)}} = \frac{y_{\max} - \eta y_{ijk} - d_y - jd_n}{x_{\max} - x_j - i \times n - d_x} \tag{24}$$

$$a_{\text{ijk(2N+1)}} = \frac{y_{\max} - \eta y_{ijk} - m - d_y - jd_n}{x_{\max} - x_j - i \times n - d_x} \tag{25}$$

Thus, the component coordinates of the nozzle can be expressed as follows:

For even $k = 2N$:

$$y - (\eta y_{ijk} + d_y + jd_n) = a_{\text{ijk(2N)}}(x - (x_j + i \times n + d_x)) \tag{26}$$

For odd $k = 2N + 1$:

$$y - (\eta y_{ijk} + m + d_y + jd_n) = a_{\text{ijk(2N+1)}}(x - (x_j + i \times n + d_x)) \tag{27}$$

According to the IC coordinates, the slope coefficients of the primary and secondary nozzles are redefined as follows:

$$a_{jk} = \frac{y_{\max} - \frac{m}{2} - \beta e - d_y - jd_n}{x_{\max} - \alpha - n - j \times f - d_x} \tag{28}$$

Hence, the IC coordinates of the nozzle are given by:

$$y - (\frac{m}{2} + \beta e + d_y + jd_n) = a_{jk}(x - (\alpha + n + j \times f + d_x)) \tag{29}$$

With respect to the feeder coordinates, the slope coefficients of the nozzle are redefined as follows:

$$a_{j\delta} = \frac{y_{\max} - (\delta - 1)d_f - d_{f0} - jd_n}{x_{\max}} \tag{30}$$

Therefore, the feeder coordinates of the nozzle are expressed as:

$$y - ((\delta - 1)d_f + d_{f0} + jd_n) = a_{j\delta}x \tag{31}$$

4. Operational Cycle of the Axis System

From the analysis of the two algorithm flowcharts in Fig. 6, the general equations for the slope coefficients of components, ICs, and feeders can be derived as follows:

Slope coefficient of the components:

$$a_{\mathrm{ij}kl(2\mathrm{N})} = \frac{y_{\max} - \eta y_{ijk} - d_y - jd_n}{x_{\max} - x_j - i \times n - d_x} \tag{32}$$

$$a_{\mathrm{ijk}(2\mathrm{N}+1)} = \frac{y_{\max} - \eta y_{ijk} - m - d_y - jd_n}{x_{\max} - x_j - i \times n - d_x} \tag{33}$$

Slope coefficient of the IC:

$$a_{jkl} = \frac{y_{\max} - \frac{m}{2} - \beta e - d_y - jd_n}{x_{\max} - \alpha - n - j \times f - d_x} \tag{34}$$

Slope coefficient of the feeder:

$$a_{j\delta} = \frac{y_{\max} - (\delta - 1)d_f - d_{f0} - jd_n}{x_{\max}} \tag{35}$$

The component coordinates, derived from the slope coefficients in (32) and (33), are as follows:

$$\begin{cases} y - (\eta y_{ijk} + d_y + jd_n) = a_{\mathrm{ij}kl(2N)}(x - (x_j + i \times n + d_x)) \\ y - (\eta y_{ijk} + m + d_y + jd_n) = a_{ijkl(2N+1)}(x - (x_j + i \times n + d_x)) \end{cases} \tag{36}$$

The IC coordinates, derived from the slope coefficient in (34), are as follows:

$$y - (\frac{m}{2} + \beta e + d_y + jd_n) = a_{jkl}(x - (\alpha + n + j \times f + d_x)) \tag{37}$$

The feeder coordinates, derived from the slope coefficient in (35), are as follows:

$$y - ((\delta - 1)d_f + d_{f0} + jd_n) = a_{j\delta l}x \tag{38}$$

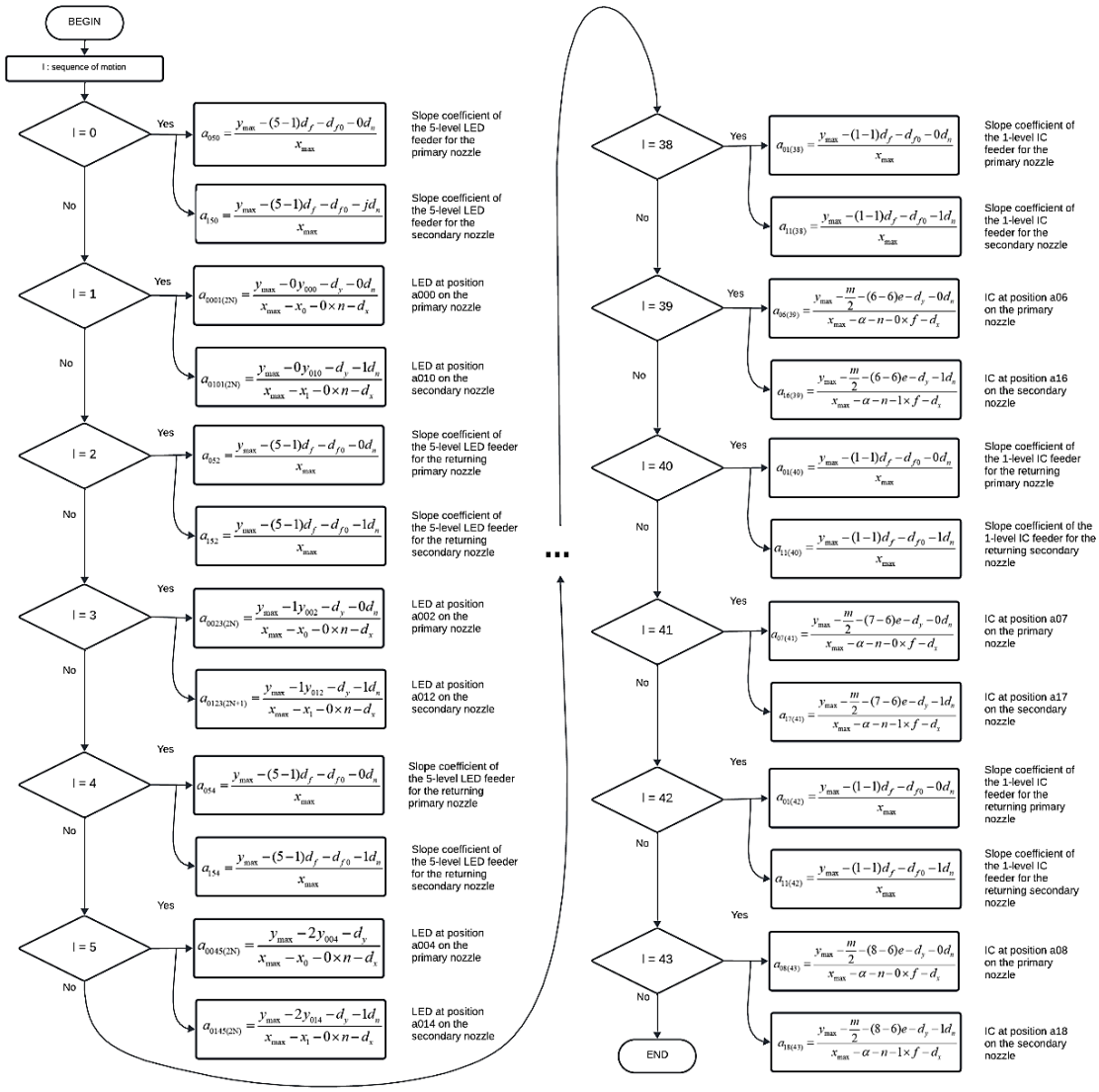

Fig. 6. Flowchart of the algorithm for the LED and IC operational cycle

Fig. 6 illustrates the overall operating cycle of the machine, in which each parameter a_{ijkl}, generalized in the previous section, is defined and applied specifically at each step of the process. The cycle is executed sequentially from $l = 0$ to $l = 43$. At each step, the coordinates and slope coefficients of the components are determined, while the two nozzles (primary and secondary) are controlled in parallel to perform the pick-and-place operations. The computational equations indicate that the placement positions are derived from the feeder parameters, displacements, and design constants, thereby ensuring precision and stability during operation.

5. Results and Discussion

To validate the calculation results, experiments were conducted on a real PCB processing model, as illustrated in Fig. 7. The system comprises a Mitsubishi R04ENCPU PLC acting as the central controller, an MR-J4W3-222B amplifier for motion control, and three servo motors. Two 200W motors are employed for movement along the X and Y axes, while a 100W motor is responsible for movement along the Z-axis. Based on the coordinate values listed in Table 1 and Table 2, the position vectors are determined. To realize the motion toward these positions, the inverse kinematics problem of the robot is solved to derive the corresponding joint angles. High-speed positioning accuracy is

maintained through the implementation of a proportional-derivative (PD) controller for the servo motors. These components, together with the experimental model setup, are depicted in Fig. 7.

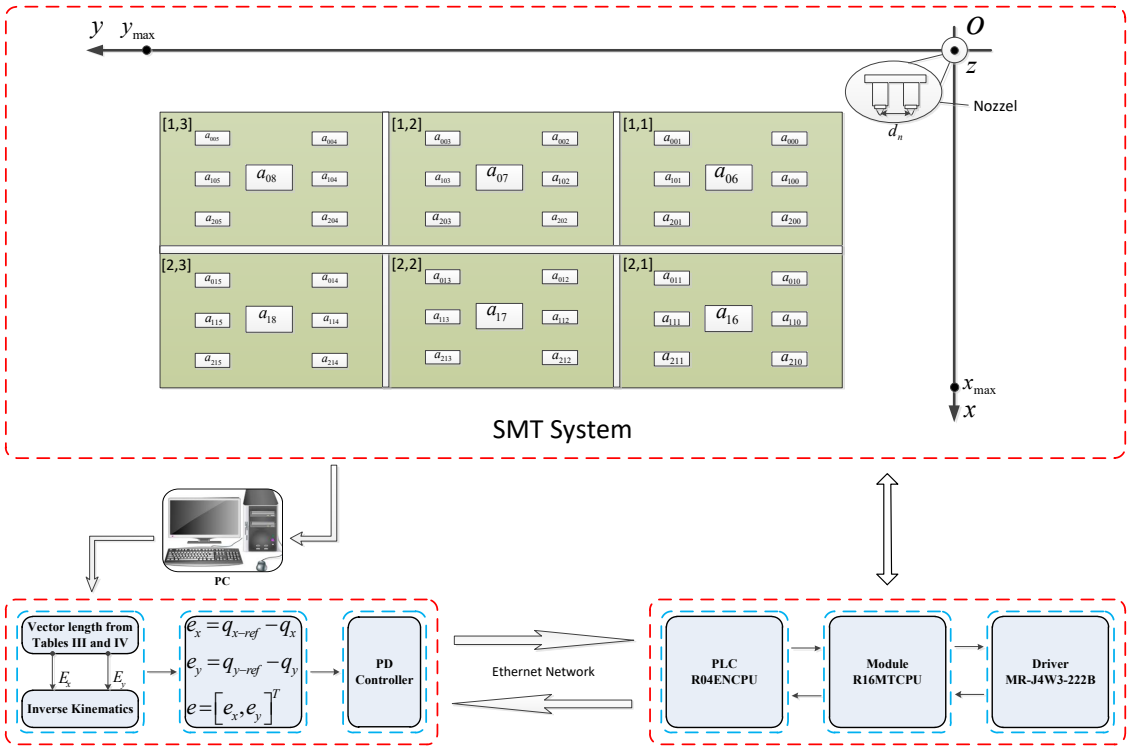

Fig. 7. Block diagram of device interconnections

From Table 1 and Table 2, the spatial length vectors corresponding to each target component were calculated. These geometric quantities were then converted into control signals for the SMT machine through inverse kinematics, ensuring that the pick-and-place system followed the correct trajectory and position. The experiment was conducted under laboratory conditions, with an average processing time of 3 minutes and 20 seconds per circuit board, as summarized in Table 3.

The authors designed a component assembly system based on SMT technology as illustrated in Fig. 2. The machine's technical parameters are defined in detail in Table 4. Based on that, all parameters were substituted into the general equations (32)–(38) to calculate and deduce the precise coordinates of the component, IC and feeder, the results of which are presented in Table 1 and Table 2.

Table 1. Component coordinates with respect to the machine coordinate system (mm)

Component Type	Table [1,1]		Table [1,2]		Table [1,3]		Table [2,1]		Table [2,2]		Table [2,3]	
	X	Y	X	Y	X	Y	X	Y	X	Y	X	Y
Led	179.725	33.616	179.725	66.616	179.725	99.616	199.975	80.616	199.975	113.616	199.975	146.616
C3	184.525	33.616	184.525	66.616	184.525	99.616	204.775	80.616	204.775	113.616	204.775	146.616
C4	189.325	33.616	189.325	66.616	189.325	99.616	209.575	80.616	209.575	113.616	209.575	146.616
R	179.725	48.52	179.725	81.52	179.725	114.52	199.975	95.52	199.975	128.52	199.975	161.52
C1	184.525	48.52	184.525	81.52	184.525	114.52	204.775	95.52	204.775	128.52	204.775	161.52
C2	189.325	48.52	189.325	81.52	189.325	114.52	209.575	95.52	209.575	128.52	209.575	161.52
IC	184.525	41.068	184.525	74.068	184.525	107.068	204.775	88.068	204.775	121.068	204.775	154.068

Table 2. Coordinates of feeders relative to the machine coordinate system (mm)

Feeder Type	Slope a		Coordinates (X,Y)	
	The primary nozzles	The secondary nozzles	The primary nozzles	The secondary nozzles
Feeder 5 Led	0.555	0.4767	(0,267)	(0,314)
Feeder 4 (Capacitor C3, C4)	0.63	0.5517	(0,222)	(0,269)
Fedder 3 (Resistor R)	0.705	0.6267	(0,177)	(0,224)
Feeder 2 (Capacitor C1, C2)	0.78	0.7017	(0,132)	(0.179)
Feeder 1 (IC)	0.855	0.7767	(0,87)	(0,134)

Table 3. Detailed evaluation of errors and success rates of the model

Trial No.	Number of Tested Circuits	Result	Notes
1	5	Completed	
2	10	Completed	
3	12	2 Faulty Circuits	The last two circuits missed components due to feeder malfunction.
4	20	3 Faulty Circuits	The first circuit missed a component due to pump malfunction. Circuits No. 11 and 12 lacked components due to feeder malfunction.
5	15	Completed	

Table 4. Parameters of the general equations (mm)

Variable	Value (mm)
$\boldsymbol{n}$	4.8
$\boldsymbol{m}$	14.904
$\boldsymbol{e}$	33
$\boldsymbol{f}$	20.25
$\boldsymbol{u}$	20.25
$\boldsymbol{y_{ijk}}$	33 (for all ijk)
$\boldsymbol{x}_{\max}$	600
$\boldsymbol{y}_{\max}$	600
$\boldsymbol{d_f}$	45
$\boldsymbol{d_{f0}}$	87
$\boldsymbol{d_x}$	179.725
$\boldsymbol{d_y}$	33.616
$\boldsymbol{d_n}$	47

The computed results in Table 1 and Table 2 are embedded directly into the Mitsubishi R04ENCPU programmable logic controller (PLC) to verify and control the machining process in the physical testbed. These data serve as input to the control program, ensuring placement accuracy during assembly [53]–[56]. The system employs an MR-J4W3-222B driver to simultaneously control three servo motors, enabling high-precision positioning and speed regulation [57]–[60]. To clarify the integration between the computational module and the control hardware, the block diagram in Fig. 7 illustrates the linkage between the generated data and the PLC.

Fig. 8 is experiment on the XY-axis trajectory moving from the origin (0,0) to the feeder 5 supplying LED components and the placement points (a_{000}= (179.725, 33.616), a_{010}= (199.975, 80.616)). The process begins at $l = 0$ and ends at $l = 1$. During this sequence, the axis departs from the coordinate origin, where the primary nozzle first moves to Feeder 5 to pick up an LED, followed by the secondary nozzle performing the same pick-up operation. Once both nozzles have acquired components, the axis moves to the LED position a_{000}, where the primary nozzle places the component. Subsequently, the secondary nozzle proceeds to place its component.

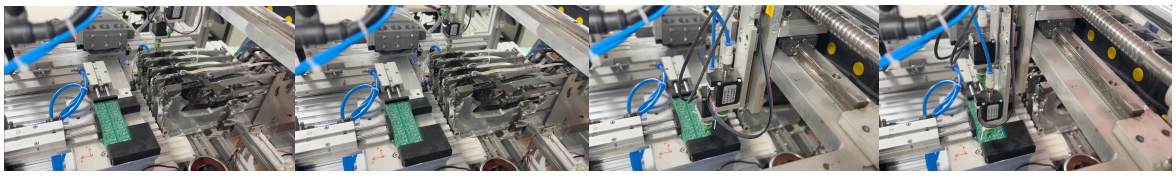

Fig. 8. Experimental illustration of the XY-axis trajectory from the origin (0,0) to Feeder 5 and the component placement positions, demonstrating the complete pick-and-place cycle for LED components

Fig. 9 is experiment on the XY-axis trajectory from Feeder 5 supplying LED components to the designated placement points (a_{002}= (179.725, 66.616), a_{012}= (199.975, 113.616)). The process runs from $l = 0$ to $l = 1$, where the axis retrieves LED components from Feeder 5 and sequentially moves to place them at the specified positions using the main and sub nozzles.

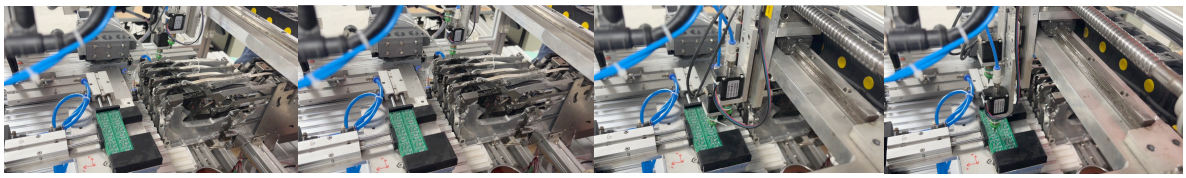

Fig. 9. Experimental illustration of the XY-axis trajectory from Feeder 5 to the component placement positions, demonstrating the complete pick-and-place cycle for LED components

Fig. 10 is experiment on the XY-axis trajectory from Feeder 1 supplying IC components to the designated placement points (a_{06} = (184.525, 41.068), a_{16} = (204.775, 88.068)). The process runs from l = 42 to l =43, where the axis retrieves IC components from Feeder 1 and sequentially moves to place them at the specified positions using the main and sub nozzles.

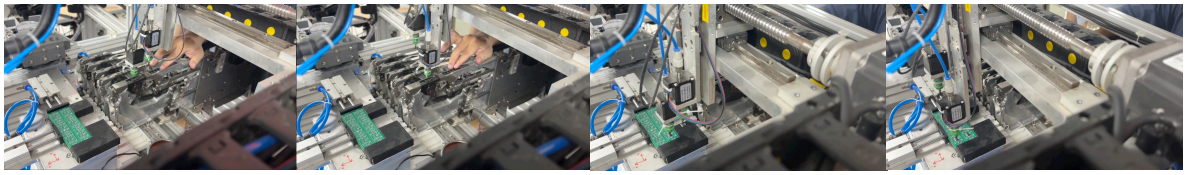

Fig. 10. Experimental illustration of the XY-axis trajectory from Feeder 1 to the component placement positions, demonstrating the complete pick-and-place cycle for IC components

Fig. 11 is final assembled PCB result with slope coefficient in Table 5. The figure illustrates the completed product after the entire fabrication process. To evaluate the reliability of the proposed coordinate determination algorithm described in Section 2, Section 3, and Section 4, five experimental runs were conducted, resulting in a total of 62 fabricated circuits. A summary of the experimental outcomes is provided in Table 3.

Experimental results from Table 3 indicate that the system achieved an accuracy of 91.94% (57/62 successful assemblies). However, in the unsuccessful trials, the primary causes were attributed to hardware malfunctions, while virtually no instances of misplacement or component deviation beyond the permissible tolerance (error ≤ 0.2 mm) were observed, as shown in Fig. 11 in compliance with the IPC-A-610 standard. This confirms the reliability of the proposed coordinate determination algorithm presented in Section 4. Compared with other approaches that typically rely on offline learning algorithms to optimize placement positions—yet lack adaptability to real-time positional variations. The method proposed in this study is developed and computed directly based on spatial coordinates and linear equations. This formulation enhances placement accuracy during operation. Future improvements could focus on enhancing hardware reliability, such as through more robust nozzle design or vision-based error correction. Furthermore, the underlying mathematical model shows potential for scalability, suggesting applicability to larger or more complex PCB layouts involving higher component density. The complete assembly process of a single circuit board is

illustrated in the accompanying demonstration video. (Link YouTube: https://youtu.be/Lbx8E54XIk8).

Table 5. Slope coefficients of components on the PCB

Component Type	Table [1,1]	Table [1,2]	Table [1,3]	Table [2,1]	Table [2,2]	Table [2,3]
	a	a	a	a	a	a
Led	1.3476	1.2691	1.1914	1.2984	1.2159	1.1334
C3	1.3632	1.2838	1.2046	1.3142	1.2307	1.1472
C4	1.3791	1.2988	1.2182	1.3303	1.2458	1.1613
R	1.3122	1.2336	1.1556	1.2611	1.1786	1.0961
C1	1.3273	1.2479	1.1684	1.2764	1.1929	1.1094
C2	1.3428	1.2625	1.1816	1.2922	1.2076	1.1231
IC	1.3466	1.2659	1.1864	1.2953	1.2118	1.1283

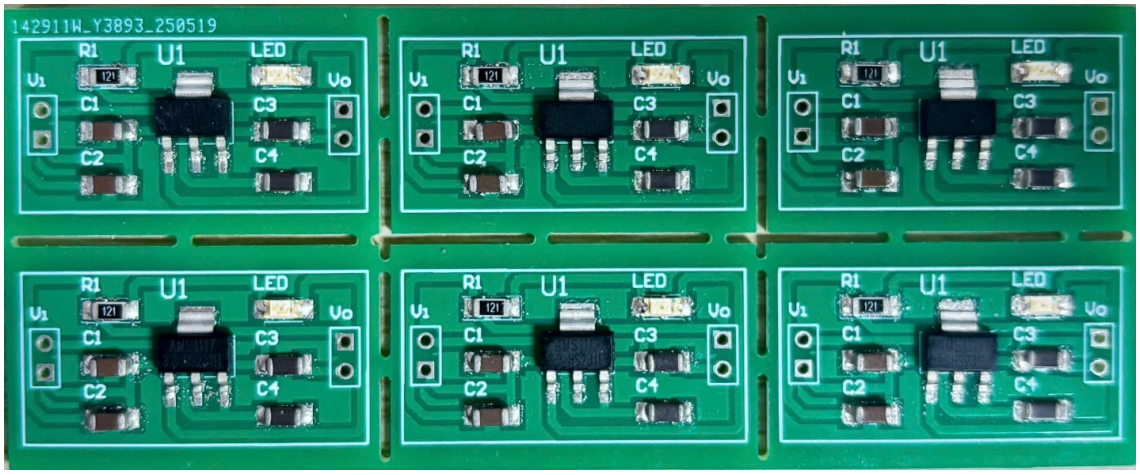

Fig. 11. The final step-down circuit after the fabrication process

6. Conclusion

This study proposed and validated a mathematical formulation for component coordinate computation in a Surface Mount Technology (SMT) placement system, aiming to enhance placement precision through deterministic coordinate transformation rather than purely heuristic trajectory tuning. Experimental evaluation on 62 printed circuit boards demonstrated that the proposed method achieved a placement accuracy of 91.94%, and importantly, no measured deviations exceeded the allowable tolerance threshold of 0.2 mm. These results confirm that the approach is not only theoretically consistent but also practically viable for improving placement reliability in real SMT production environments.

Despite these promising outcomes, several limitations should be recognized to ensure a balanced interpretation of the findings. First, the overall system performance remains partially constrained by hardware characteristics, particularly the use of dual nozzles and conventional feeders, which may introduce mechanical variability and limit repeatability under high-speed operation. Second, from a methodological standpoint, the proposed model has not yet been extensively verified across a wider range of PCB geometries, component densities, and layout complexities. Moreover, the current work does not include benchmarking against alternative coordinate computation or optimization approaches—such as heuristic-based strategies, Genetic Algorithms, or Ant Colony Optimization—which limits the ability to quantitatively position the method relative to established techniques in terms of cycle time reduction, setup time, and robustness.

Future research should therefore advance in two complementary directions. On the hardware side, system-level improvements such as upgrading the vacuum pump, implementing electrically driven

feeders, and improving nozzle precision are expected to reduce residual mechanical disturbances and enhance repeatability. On the methodological side, the proposed formulation should be extended and evaluated under more diverse PCB designs, scaled to larger production scenarios, and systematically compared against state-of-the-art algorithms and coordinate error compensation strategies. Addressing these aspects will not only improve accuracy and stability but also strengthen the industrial generalizability of the method and provide deeper insights into its applicability for next-generation SMT placement optimization.

Author Contribution: All authors contributed equally to the main contributor to this paper. All authors read and approved the final paper.

Conflicts of Interest: The authors declare no conflict of interest.

References

[1] R. P. Prasad, *Surface mount technology: Principles and practice.* Dordrecht, The Netherlands: Springer Netherlands, 2012, https://books.google.co.id/books?id=hqDdBgAAQBAJ.

[2] R. P. Prasad, "Introduction to surface mount technology," in *Surface mount technology: Principles and practice,* R. P. Prasad, Ed. Boston, MA, USA: Springer US, 1997, ch. 1, pp. 3–50, https://doi.org/10.1007/978-1-4615-4084-7_1.

[3] P. Marcoux, *Fine pitch surface mount technology: Quality, design, and manufacturing techniques.* Boston, MA, USA: Springer US, 2013, https://books.google.co.id/books?id=J1PVBwAAQBAJ.

[4] H. W. Markstein, "SMT advantages," in *The electronics assembly handbook,* F. Riley, Ed. Berlin, Heidelberg, Germany: Springer Berlin Heidelberg, 1988, ch. 28, pp. 156–163, https://doi.org/10.1007/978-3-662-13161-9_28.

[5] W. D. Bjorndahl, K. Selk, and W. Chen, "Surface mount technology: Capabilities and requirements," in *Proceedings of the 1997 IEEE Aerospace Conference,* vol. 4, Big Sky, MT, USA, Feb. 1997, pp. 285–291, https://doi.org/10.1109/AERO.1997.577515.

[6] G. Derman, "The impact of surface mount technology on electronics manufacturing," *Microelectronics Journal,* vol. 17, no. 2, pp. 5–11, Mar. 1986, https://doi.org/10.1016/S0026-2692(86)80002-7.

[7] R. J. Pryputniewicz, D. Rosato, and C. Furlong, "Measurements and simulation of SMT components," *Microelectronics International,* vol. 20, no. 1, pp. 13–16, 2003, https://doi.org/10.1108/13565360310455463.

[8] T. He, D. Li, and S. W. Yoon, "A multi-phase planning heuristic for a dual-delivery SMT placement machine optimization," *Robotics and Computer-Integrated Manufacturing,* vol. 47, pp. 85–94, Oct. 2017, https://doi.org/10.1016/j.rcim.2016.11.006.

[9] S. Cao, I. Parviziomran, S. Park, and D. Won, "Statistical analysis for component shift in pick and place process of surface mount technology," *Procedia Manufacturing,* vol. 38, pp. 217–224, 2019, https://doi.org/10.1016/j.promfg.2020.01.029.

[10] M. Cauwe, B. Vandevelde, C. Nawghane, M. Van De Slyeke, E. Bosman, J. Verhegge, A. Coulon, and S. Heltzel, "High-density interconnect technology assessment of printed circuit boards for space applications," *IMAPS Proceedings,* vol. 17, no. 3, pp. 79–88, Jul. 2020, https://doi.org/10.4071/imaps.1212898.

[11] M.-K. Shih, Y.-W. Huang, and G.-S. Lin, "Next-generation high-density PCB development by fan-out RDL technology," *IEEE Transactions on Device and Materials Reliability,* vol. 22, no. 2, pp. 296–305, Jun. 2022, https://doi.org/10.1109/TDMR.2022.3174604.

[12] T. Swirbel, A. Naujoks, and M. Watkins, "Electrical design and simulation of high density printed circuit boards," *IEEE Transactions on Advanced Packaging,* vol. 22, no. 3, pp. 416–423, Aug. 1999, https://doi.org/10.1109/6040.784495.

[13] H.-M. Tong, "Microelectronics packaging: Present and future," *Materials Chemistry and Physics,* vol. 40, no. 3, pp. 147–161, Apr. 1995, https://doi.org/10.1016/0254-0584(94)01462-P.

[14] A. Alwaidh, M. Sharp, and P. French, "Laser processing of rigid and flexible PCBs," *Optics and Lasers in Engineering,* vol. 58, pp. 109–113, Jul. 2014, https://doi.org/10.1016/j.optlaseng.2014.02.006.

[15] M. Poliks, J. Turner, K. Ghose, Z. Jin, M. Garg, Q. Gui, A. Arias, Y. Kahn, M. Schadt, and F. Egitto, "A wearable flexible hybrid electronics ECG monitor," in *Proceedings of the 2016 IEEE 66th Electronic Components and Technology Conference (ECTC),* Las Vegas, NV, USA, May–Jun. 2016, pp. 1623–1631, https://doi.org/10.1109/ECTC.2016.395.

[16] L. Kong, W. Li, T. Zhang, H. Ma, Y. Cao, K. Wang, Y. Zhou, A. Shamim, L. Zheng, X. Wang, and W. Huang, "Wireless technologies in flexible and wearable sensing: From materials design, system integration to applications," *Advanced Materials,* vol. 36, no. 27, p. 2400333, Jul. 2024, https://doi.org/10.1002/adma.202400333.

[17] T. Shimoto, K. Matsui, K. Kikuchi, Y. Shimada, and K. Utsumi, "New high-density multilayer technology on PCB," *IEEE Transactions on Advanced Packaging,* vol. 22, no. 2, pp. 116–122, May 1999, https://doi.org/10.1109/6040.763181.

[18] X. Qi, B. Zhou, and Y. En, "Effect of solder joint parameter on vibration fatigue reliability of high density PCB assembly," in *Proceedings of the 2011 International Conference on Quality, Reliability, Risk, Maintenance, and Safety Engineering,* Jun. 2011, pp. 514–517, https://doi.org/10.1109/ICQR2MSE.2011.5976665.

[19] M. I. Khan, H. Dong, F. Shabbir, and R. Shoukat, "Embedded passive components in advanced 3D chips and micro/nano electronic systems," *Microsystem Technologies,* vol. 24, no. 2, pp. 869–877, Feb. 2018, https://doi.org/10.1007/s00542-017-3586-3.

[20] C. Cantone and A. Faro, "Overview of automated optical inspection and edge AI inference system solutions," in *Artificial Intelligence-Based Smart Vision for Quality Inspection,* Boca Raton, FL, USA: CRC Press, 2023, ch. 7, https://doi.org/10.1201/9781003478713-7.

[21] S. Cao, I. Parviziomran, H. Yang, S. Park, and D. Won, "Prediction of component shifts in pick and place process of surface mount technology using support vector regression," *Procedia Manufacturing,* vol. 39, pp. 210–217, 2019, https://doi.org/10.1016/j.promfg.2020.01.316.

[22] A. R. Gokulnath, S. Chandrakumar, and T. D. Sudhakar, "Open source automated SMD pick and place machine," *Procedia Computer Science,* vol. 133, pp. 872–878, 2018, https://doi.org/10.1016/j.procs.2018.07.107.

[23] T. He, D. Li, and S. W. Yoon, "A heuristic algorithm to balance workloads of high-speed SMT machines in a PCB assembly line," *Procedia Manufacturing,* vol. 11, pp. 1790–1797, 2017, https://doi.org/10.1016/j.promfg.2017.07.316.

[24] M. H. J. Romanycia and F. J. Pelletier, "What is a heuristic?," *Computational Intelligence,* vol. 1, no. 1, pp. 47–58, Jan. 1985, https://doi.org/10.1111/j.1467-8640.1985.tb00058.x.

[25] W. J. Clancey, "Heuristic classification," *Artificial Intelligence,* vol. 27, no. 3, pp. 289–350, Dec. 1985, https://doi.org/10.1016/0004-3702(85)90016-5.

[26] B. Andres, A. Biewer, J. Romero, C. Haubelt, and T. Schaub, "Improving coordinated SMT-based system synthesis by utilizing domain-specific heuristics," in *Logic Programming and Nonmonotonic Reasoning,* F. Calimeri, G. Ianni, and M. Truszczynski, Eds. Cham, Switzerland: Springer International Publishing, 2015, pp. 55–68, https://doi.org/10.1007/978-3-319-23264-5_6.

[27] J. Díaz, J. I. Hidalgo, F. Fernández, O. Garnica, and S. López, "Improving SMT performance: An application of genetic algorithms to configure resizable caches," in *Proceedings of the 11th Annual Conference Companion on Genetic and Evolutionary Computation Conference: Late Breaking Papers,* Montreal, QC, Canada, 2009, pp. 2029–2034, https://doi.org/10.1145/1570256.1570271.

[28] T. V. Mathew, *Genetic algorithm.* Mumbai, India: Indian Institute of Technology Bombay, 2012, https://datajobs.com/data-science-repo/Genetic-Algorithm-Guide-%5BTom-Mathew%5D.pdf.

[29] A. Niewiadomski, W. Penczek, and J. Skaruz, "Genetic algorithm to the power of SMT: A hybrid approach to web service composition problem," in *Proceedings of the 2014 International Conference on Advanced Service Computing (SERVICE COMPUTATION 2014),* Venice, Italy, May 2014, pp. 44–48, https://personales.upv.es/thinkmind/SERVICE_COMPUTATION/SERVICE_COMPUTATION_2014/service_computation_2014_2_30_10035.html.

[30] Q. Guo, M. Zhao, and L. Wei, "SMT solder joint's shape and location optimization using genetic algorithm with neural networks in high acceleration condition," in *Proceedings of the 2004 24th International Conference on Microelectronics,* vol. 2, May 2004, pp. 709–712, https://doi.org/10.1109/ICMEL.2004.1314929.

[31] L. P. Khoo and T. K. Ng, "A genetic algorithm-based planning system for PCB component placement," *International Journal of Production Economics,* vol. 54, no. 3, pp. 321–332, May 1998, https://doi.org/10.1016/S0925-5273(98)00010-3.

[32] H. Chen and H. Zhang, "A study on optimization of SMT machine--based on ant colony algorithm," in *Proceedings of the 2021 International Conference on Information Control, Electrical Engineering and Rail Transit (ICEERT),* Oct.–Nov. 2021, pp. 9–13, https://doi.org/10.1109/ICEERT53919.2021.00010.

[33] M. Dorigo and C. Blum, "Ant colony optimization theory: A survey," *Theoretical Computer Science,* vol. 344, no. 2–3, pp. 243–278, Nov. 2005, https://doi.org/10.1016/j.tcs.2005.05.020.

[34] M. Dorigo and K. Socha, "An introduction to ant colony optimization," in *Handbook of Approximation Algorithms and Metaheuristics: Methodologies and Traditional Applications, vol. 1,* 2nd ed., T. F. Gonzalez, Ed. Boca Raton, FL, USA: Chapman and Hall/CRC, 2018, ch. 23, https://doi.org/10.1201/9781351236423-23.

[35] X. Du and G. Yu, "Optimizing the performance of chip shooter machine based on ant colony algorithm," *Applied Mechanics and Materials,* vol. 224, pp. 47–50, Nov. 2012, https://doi.org/10.4028/www.scientific.net/AMM.224.47.

[36] J. Jiang, Z. Du, C. Liu, and Z. Kun, "Ant colony algorithms with characteristic of clustering for surface mount technology optimization," in *Proceedings of the 2010 6th International Conference on Wireless Communications Networking and Mobile Computing (WiCOM),* Sep. 2010, pp. 1–4, https://doi.org/10.1109/WICOM.2010.5601320.

[37] M. P. Cooper, C. A. Griffiths, K. T. Andrzejewski, and C. Giannetti, "Motion optimisation for improved cycle time and reduced vibration in robotic assembly of electronic components," *AIMS Electronics and Electrical Engineering,* vol. 3, no. 3, pp. 274–289, Aug. 2019, https://doi.org/10.3934/ElectrEng.2019.3.274.

[38] X. Shan, Y. Li, H. Liu, and T. Huang, "Residual vibration reduction of high-speed pick-and-place parallel robot using input shaping," *Chinese Journal of Mechanical Engineering,* vol. 35, no. 1, p. 16, Feb. 2022, https://doi.org/10.1186/s10033-022-00679-3.

[39] M. Štrimaitis, R. Urbanavičius, A. Kilikevičius, M. Jurevičius, V. Striška, and A. Trumpa, "Evaluation of dynamics and positioning accuracy of robotic system operating in heavy loaded high speed conditions," *Journal of Measurements in Engineering,* vol. 1, no. 1, pp. 28–34, Mar. 2013, https://www.extrica.com/article/14410.

[40] K. K. Kode, "Effect of Humidity and Nozzle Cleanliness on SMT Mounting Success Rate," Master's thesis, State University of New York at Binghamton, 2024, https://www.proquest.com/dissertations-theses/effect-humidity-nozzle-cleanliness-on-smt/docview/3082123306/se-2.

[41] L. Liu, C. Zhang, and Z. Chen, "Effects of pickup variations on chip placement in SMT by finite element modeling," in *Proceedings of the 2022 IEEE 24th Electronics Packaging Technology Conference (EPTC),* Dec. 2022, pp. 684–688, https://doi.org/10.1109/EPTC56328.2022.10013286.

[42] S. E. Raasch and S. K. Reinhardt, "The impact of resource partitioning on SMT processors," in *Proceedings of the 12th International Conference on Parallel Architectures and Compilation Techniques (PACT),* 2003, p. 15, https://dl.acm.org/doi/10.5555/942806.943858.

[43] A. Al-Refaie, "Optimizing SMT performance using comparisons of efficiency between different systems technique in DEA," *IEEE Transactions on Electronics Packaging Manufacturing,* vol. 32, no. 4, pp. 256–264, Oct. 2009, https://doi.org/10.1109/TEPM.2009.2029238.

[44] J. Han and Y. Seo, "Mechanism to minimise the assembly time with feeder assignment for a multi-headed gantry and high-speed SMT machine," *International Journal of Production Research,* vol. 55, no. 10, pp. 2930–2949, 2017, https://doi.org/10.1080/00207543.2016.1229071.

[45] H. Tae and B.-I. Kim, "Feeder re-assign problem in a surface mount device with a piano-type multi-headed gantry," *Industrial Engineering and Management Systems,* vol. 12, no. 4, pp. 330–335, Dec. 2013, https://doi.org/10.7232/iems.2013.12.4.330.

[46] W. Wang, P. C. Nelson, and T. M. Tirpak, "Optimization of high-speed multistation SMT placement machines using evolutionary algorithms," *IEEE Transactions on Electronics Packaging Manufacturing,* vol. 22, no. 2, pp. 137–146, Apr. 1999, https://doi.org/10.1109/6104.778173.

[47] F. Devernay and O. Faugeras, "Straight lines have to be straight," *Machine Vision and Applications,* vol. 13, no. 1, pp. 14–24, Aug. 2001, https://doi.org/10.1007/PL00013269.

[48] T. L. Nguyen, S.-K. Ro, and J.-K. Park, "Study of ball screw system preload monitoring during operation based on the motor current and screw-nut vibration," *Mechanical Systems and Signal Processing,* vol. 131, pp. 18–32, Sep. 2019, https://doi.org/10.1016/j.ymssp.2019.05.036.

[49] F.-Y. Pai, T.-M. Yeh, and Y.-H. Hung, "Analysis on accuracy of bias, linearity and stability of measurement system in ball screw processes by simulation," *Sustainability,* vol. 7, no. 11, pp. 15464–15486, 2015, https://doi.org/10.3390/su71115464.

[50] T. Zhong, R. Nagamune, D. Bao, and W. Tang, "Gain-scheduling robust control with guaranteed stability for ball screw drives with uncertain load mass and varying resonant modes," *Precision Engineering,* vol. 80, pp. 198–207, Mar. 2023, https://doi.org/10.1016/j.precisioneng.2022.12.006.

[51] V. Pandhare, M. Miller, G. W. Vogl, and J. Lee, "Ball screw health monitoring with inertial sensors," *IEEE Transactions on Industrial Informatics,* vol. 19, no. 6, pp. 7323–7334, Jun. 2023, https://doi.org/10.1109/TII.2022.3210999.

[52] O. Horejs, "Thermo-mechanical model of ball screw with non-steady heat sources," in *Proceedings of the 2007 International Conference on Thermal Issues in Emerging Technologies: Theory and Application,* Jan. 2007, pp. 133–137, https://doi.org/10.1109/THETA.2007.363424.

[53] Yashika, A. Patra, and N. S. Das, "Human-machine interaction in industrial automation: Gesture-based PLC control," in *Proceedings of the 2024 15th International Conference on Computing Communication and Networking Technologies (ICCCNT),* Jun. 2024, pp. 1–7, https://doi.org/10.1109/ICCCNT61001.2024.10726180.

[54] A. Milecki, R. Regulski, D. Sędziak, P. Owczarek, and Z. Proch, "Application of computer system in control and programming of a robotized soldering station," *MATEC Web of Conferences,* vol. 252, p. 02008, Jan. 2019, https://doi.org/10.1051/matecconf/201925202008.

[55] K. Prabhu, N. Mahesh, P. K. Muthu, G. Karthikeyan, and C. A. Bhuvaneswari, "PLC based colour sorting and pick and place system for industrial automation," in *Proceedings of the 2023 Third International Conference on Ubiquitous Computing and Intelligent Information Systems (ICUIS),* Sep. 2023, pp. 105–110, https://doi.org/10.1109/ICUIS60567.2023.00026.

[56] J. Wang, "Stable control of hydraulic robotic arm during operation using PLC technology," *Automatika,* vol. 66, no. 2, pp. 300–305, 2025, https://doi.org/10.1080/00051144.2025.2474279.

[57] V. Hristov, "Control of single-axis servo motor drive with PLC controller," in *Proceedings of the 2025 14th Mediterranean Conference on Embedded Computing (MECO),* Jun. 2025, pp. 1–8, https://doi.org/10.1109/MECO66322.2025.11049233.

[58] K. Hristov and V. Hristov, "Servo drive control system," in *Proceedings of the 2023 International Scientific Conference on Computer Science (COMSCI),* Sep. 2023, pp. 1–6, https://doi.org/10.1109/COMSCI59259.2023.10315927.

[59] J. Wang, H. Wang, D. Deng, T. Wang, D. Xia, and W. Qi, "Research on the control system of strawberry picking robot based on Halcon vision and multi-axis collaborative control of Mitsubishi PLC," in *Proceedings of the 2025 IEEE 2nd International Conference on Deep Learning and Computer Vision (DLCV),* Jun. 2025, pp. 1–5, https://doi.org/10.1109/DLCV65218.2025.11088524.

[60] S. Y. Lei, "Servo-control system design of automatic production line based on PLC and HMI," *Applied Mechanics and Materials,* vol. 457–458, pp. 1381–1385, 2014, https://doi.org/10.4028/www.scientific.net/AMM.457-458.1381.